PCCP

On the mechanism of soot nucleation. II. E-bridge formation at PAH bay

Journal:	*Physical Chemistry Chemical Physics*
Manuscript ID	CP-ART-05-2020-002554.R1
Article Type:	Paper
Date Submitted by the Author:	09-Jun-2020
Complete List of Authors:	Semenikhin, Alexander; Samarskij nacional'nyj issledovatel'skij universitet imeni akademika S P Koroleva Savchenkova, Anna; Samara National Research University, Chechet, Ivan; Samarskij nacional'nyj issledovatel'skij universitet imeni akademika S P Koroleva, Matveev, Sergei; Samarskij nacional'nyj issledovatel'skij universitet imeni akademika S P Koroleva, Frenklach, Michael; University of California at Berkeley, Department of Mechanical Engineering Mebel, Alexander; Florida International University, Chemistry and Biochemistry

On the mechanism of soot nucleation. II. E-bridge formation at PAH bay†

Alexander S. Semenikhin[a], Anna S. Savchenkova[a,*], Ivan V. Chechet[a], Sergey G. Matveev[a], Michael Frenklach[b,*], and Alexander M. Mebel[a,c,*]

[a] Samara National Research University, Samara, 443086, Russia. E-mail: paramonovaanna@mail.ru

[b]Department of Mechanical Engineering, University of California at Berkeley, Berkeley, California, 94720-1740, USA. E-mail: frenklach@berkeley.edu

[c]Department of Chemistry and Biochemistry, Florida International University, Miami, Florida, 33199, USA. E-mail: mebela@fiu.edu

Abstract. The recently proposed mechanism of soot nucleation (Phys. Chem. Chem. Phys., 2020, 22, 5314–5331) based upon the formation of a rotationally-activated dimer in collision of aromatic molecule and radical leading to a stable, doubly-bonded E-bridge between them, rooted in the existence of a five-member ring on the molecule edge, has been further investigated with a focus on the 5-6 E-bridge forming in reaction of a PAH cycopenta group with a bay site of another PAH. As a prototype reaction of this kind, we examined the reaction between 4-phenanthrenyl and acenaphthylene and, to project these results to larger aromatic structures, we also explored the size effect of the E-bridge forming reactions by computing the 1-naphthyl + acenaphthylene system and comparing these results with the prior results for pyrenyl + acepyrene. The two systems have been studies by high-level G3(MP2,CC)//B3LYP/6-311G(d,p) ab initio calculations of their potential energy surfaces combined with RRKM-Master Equation calculations of reaction rate constants. With PAH monomers of similar sizes involved, the formation of the E-bridge structures at the bay radical sites appeared to be faster and lead to the increased nucleation rates as compared to the zigzag-forming ones. A model combining both the bay and zigzag rotationally-induced formation of E-bridges successfully reaches the level of nucleation fluxes comparable to those of the irreversible pyrene dimerization thus affirming the rotationally-activated dimerization as a feasible mechanism for soot particle nucleation.

† *Electronic Supplementary Information (ESI) available: Rate coefficients of the most relevant reactions considered. See DOI:*

Introduction

Products of incomplete combustion of fossil fuels contain aerosol particles of soot, which can have a significant impact on the climate and clean air. Small soot particles of 0.5-2 microns in size are retained in the lungs and respiratory tract, causing various diseases. In addition, soot adsorbs heavy polycyclic aromatic hydrocarbons (PAHs) and hence, it is often believed that soot like the PAHs is also carcinogenic. These societal concerns, among other factors, motivate the continuous efforts in establishing the mechanism of soot formation.

Formation of soot in hydrocarbon combustion is a complex process[1] and one of its significant parts is nucleation.[2,3] The physical mechanism controlling the emergence of the very initial soot nuclei has been increasingly researched in recent years. The main ideas and their shortcomings were recently reviewed by Frenklach and Mebel,[4] who then suggested a new mechanism based on HACA and rotational activation of colliding PAH: A PAH radical, formed by H-abstraction, collides with another PAH ensuing internal rotation of a temporary-lived adduct; during the lifetime of the rotationally-activated dimer, the reaction between the radical site of the former and a cyclopenta group present on the edge of the latter forms a stable, covalently-bonded bridge.

A specific reaction examined in Ref. 4 was initiated by a radical formed on a PAH zigzag edge forming a bridge composed of two five-member rings sharing a common bond; this bridge, shown in Fig. 1, was termed E-bridge. The possibility of other, similar or even more efficient reactions was suggested by Frenklach and Mebel.[4] Indeed, such a case is presented here: a reaction initiated by a bay-radical site forming a bridge composed of a bond-sharing five- and six-member ring structure (Fig. 1). To distinguish the two bridge structures, we will refer to them as “5-5” and “5-6” E-bridges, respectively.

The focus on the 5-5 E-bridges in Ref. 4 originated from considering a series of PAH stabilomers,[5,6] namely, pyrene, coronene, circumcoronene, etc., whose edges are predominately zigzag sites. However, theoretical considerations of PAH growth[2,5] and experimental evidence[7] suggest that the formation of the PAH stabilomer sequence should be accompanied by “intermediate” structures, including those with bay sites. For instance, site-resolved kinetic Monte-Carlo (KMC) simulations for a well-studied flame,[8] the one used in the prior[4] and present studies, show that over half of the forming PAH structures contain bay edge sites (Fig. 2).

In the present study, we focus therefore on the 5-6 E-bridge forming in reaction of a PAH cycopenta group with a bay site of another PAH. As a prototype reaction of this kind, we examine the reaction between 4-phenanthrenyl and acenaphthylene. To project these results to larger aromatic structures, we examine the size effect of the E-bridge forming reactions by computing the 1-naphthyl + acenaphthylene system and compare these new results with those of the pyrenyl

+ acepyrene one explored in the prior study.[4] We begin the presentation with the quantum-chemical and reaction-rate calculations, and will follow with the analysis of nucleation kinetics employing the theoretical framework of the prior study.[4]

Calculation Methods

Quantum Chemistry

Geometries of the reactants, products, intermediates, and transition states in the considered reactions were optimized using the density functional theory (DFT) B3LYP method with the 6-311G(d,p) basis set.[9,10] Vibrational frequencies were calculated at the same B3LYP/6-311G(d,p) level of theory in order to obtain zero-point vibrational energy (ZPE) corrections and to be utilized in rate constant calculations. All DFT calculations were performed using the GAUSSIAN 09 software package.[11] Single-point energies were then refined using two versions of the combined model chemistry G3(MP2,CC) scheme.[12–14] In the first version, the energy was evaluated as

E[G3(MP2,CC)] = E[CCSD(T)/6-311G(d,p)] + E[MP2/G3Large)] – E[MP2/6-311G(d,p)] + ZPE[B3LYP/6-311G(d,p)]

where the coupled clusters CCSD(T)/6-311G(d,p) energy is augmented by the basis set correction E[MP2/G3Large)] – E[MP2/6-311G(d,p)] computed at the 2nd-order Möller-Plessett perturbation theory level. The second version of the G3(MP2,CC) approach used the coupled clusters energy with a smaller 6-31G(d) basis set:

E[G3(MP2,CC)] = E[CCSD(T)/6-31G(d)] + E[MP2/G3Large)] – E[MP2/6-31G(d)] + ZPE[B3LYP/6-311G(d,p)]

For the smaller acenaphthylene + 1-naphthyl system both versions of the G3(MP2,CC) scheme were tested. The unsigned average difference in relative energies computed by the two versions was only 0.27 kcal/mol, with the largest deviation of 0.41 kcal/mol. Therefore, for the larger acenaphthylene + 4-phenanthrenyl system, we employed only the less demanding approach based on CCSD(T) energies with the smaller 6-31G(d) basis set. This less expensive G3(MP2,CC) version was also employed for variational calculations of the entrance channel of the acenaphthylene + 1-naphthyl reaction (*vide infra*). The spin-restricted (R) CCSD(T) and MP2 calculations (open-shell, RO, for radicals) were carried out using the MOLPRO 2010 software package.[15]

Reaction Rates Constants

The computed energies and molecular parameters were utilized in calculations of temperature- and pressure-dependent rate constants using the Rice-Ramsperger-Kassel-Marcus Master Equation (RRKM-ME) approach.[16] The MESS software package[17] was employed for the

RRKM-ME calculations. Partition functions and densities of states for local mimima and numbers of states for transition states were generally computed within the Rigid-Rotor, Harmonic-Oscillator (RRHO) model, whereas low-frequency normal modes corresponding to internal rotations were treated as hindered rotors. The potentials for hindered rotors were evaluated at the B3LYP/6-311G(d,p) level of theory. For the acenaphthylene + 1-naphthyl reaction, which appeared to have a submerged entrance barrier preceded by a van der Waals reactant complex, variational transition state theory was used to calculate the entrance channel rate constant. The minimal potential energy profile (MEP) in the vicinity of the submerged barrier was probed by intrinsic reaction coordinate (IRC) calculations and ten structures along the MEP were considered as transition state candidates in the RRKM-ME calculations. The IRC MEP and vibrational frequencies of the candidate structures were calculated at the B3LYP/6-311G(d,p) level and their single-point energies were refined using the CCSD(T)/6-31G(d)-based G3(MP2,CC) scheme. The Lennard-Jones parameters ε and σ for hydrocarbons were adapted from similar-size molecules in the work of Wang and Frenklach,[18] whereas the parameters for the bath gas (N_2) were taken from the papers by Vishnyakov et al.[19,20] The collisional energy transfer parameters in RRKM-ME calculations were described within the "exponential down" model,[21] where the temperature dependence of the parameter α for the deactivating wing of the energy transfer function was expressed as $\alpha(T) = \alpha_{300}\ (T/300)^n$, where $n = 0.85$ and $\alpha_{300} = 247$ cm^{-1} are "universal" values proposed by Jasper and Miller for hydrocarbons.[22]

Nucleation Kinetics

The analysis of nucleation fluxes was performed for the same conditions as used in the prior study[4] for a burner-stabilized stagnation flame:[8] 16.3% C_2H_4–23.7% O_2–Ar, cold gas velocity 8.0 cm/s, and burner-to-stagnation surface separation 0.8 cm. The gas-phase composition of the flame was computed using Cantera[23] with the Appel *et al.* (ABF) model.[24] Our selection of the ABF model should not affect the conclusions of the present study in light of the following considerations: (a) the ABF model is validated against a series of sooting flames, (b) the present analysis employs just a few primary species profiles, and (c) the present objective is an-order of magnitude analysis. The computed flame temperature and the concentration profiles of gaseous species (H, H_2, acenaphthylene, phenanthrene, pyrene, etc.) were supplied into a Matlab code describing the nucleation kinetics by a system of ordinary differential equations. The latter were solved from a flame time of 1 ms, corresponding to a flame temperature of 1412 K, for a duration of 10 ms. Additional, Kinetic Monte-Carlo (KMC) simulations were performed for the same flame using the code of Whitesides and Frenklach[25] with an updated reaction model.[26]

Results and Discussion

Potential energy surfaces for the reaction of acenaphthylene with 1-naphthyl and 4-phenanthrenyl radicals

Calculated potential energy surfaces for the reactions of acenaphthylene with 1-naphthyl and 4-phenanthrenyl radicals are illustrated in Figure 3, where the acepyrene + pyrenyl PES[4] is also shown for comparison. The mechanisms of all three reactions appear to be similar. They begin with addition of acenaphthylene (acepyrene) to the radical site forming the initial intermediate W1. In the acenaphthylene + 4-phenanthrenyl and acepyrene + pyrenyl reactions, the entrance barriers are low, ~1 kcal/mol, whereas in the acenaphthylene + 1-naphthyl reaction, the barrier is submerged, at -1.7 kcal/mol relative to the reactants, and is preceded by a reactant van der Waals complex residing at -2.4 kcal/mol. The adduct W1 containing a C-C covalent bond is stabilized by 48.0, 40.0, and 45.1 kcal/mol for acenaphthylene +1-naphthyl, acenaphthylene + 4-phenanthrenyl, and acepyrene + pyrenyl, respectively. Next, W1 can either directly eliminate a hydrogen atom from the five-member ring adjacent to the new C-C bond forming products P2, or rearrange to E-bridged structures W2. In turn, W2 can lose an H atom from the former aryl moiety producing the E-bridged bound products P1. The W1 $\rightarrow$ W2 $\rightarrow$ P1 + H pathway is clearly preferable energetically over the direct H loss W1 $\rightarrow$ P2 + H. The E-bridged product P2 in the acenaphthylene + 4-phenanthrenyl reaction is peculiar because the bridge connecting two PAHs here consists of a five-member ring (from the acenaphthylene reactant) and a new six-member ring formed on the bay edge of the phenanthrene skeleton. In the acenaphthylene + 1-naphthyl and acepyrene + pyrenyl reactions, the E-bridge involves two five-member ring, one of which is formed on the zigzag edge of the attacked aryl radical. While the energetics of the three considered reactions are qualitatively similar, there are noticeable quantitative differences. First, the reaction exothermicities both for the formation of the E-bridged product P1 and the C-C covalently bound product P2 slightly increase with the size of the reacting PAH species, from 23.1 to 24.9 kcal/mol (P1) and from 11.3 to 13.5 kcal/mol (P2) going from acenaphthylene + 1-naphthyl to acepyrene + pyrenyl. Also, when the E-bridge is made on the bay edge from a five-member ring and a six-member ring, the formation of P1 becomes even more favorable; it is computed to be exothermic by 26.2 kcal/mol for acenaphthylene + 4-phenanthrenyl compared to 23.1 kcal/mol for the system of a similar size, acenaphthylene + 1-naphthyl, where the E-bridge is formed from two five-member rings on the zigzag edge. Moreover, the preference for the formation of P1 over P2 also increases in the acenaphthylene + 4-phenanthrenyl reaction, where the energy difference between the two products is 20.7 kcal/mol compared to 11.8 and 11.4 kcal/mol for acenaphthylene + 1-naphthyl and acepyrene + pyrenyl, respectively. In summary, from the reaction energetics alone, one can conclude that the propensity to form an E-bridged PAH dimer when a five-member ring

on the edge of one PAH attacks another PAH radical should increase with the PAH size and when a bay edge of the PAH radical is involved instead of a zigzag edge. These trends can be understood more quantitatively by looking at the forward and reverse reaction rate constants.

Rate constants and equilibrium constants

Figure 4 shows calculated rate constants of the three reactions in forward and reverse directions at 1 atm. Let us begin with Fig. 4(a) illustrating the forward reaction. Clearly, the acenaphthylene + 1-naphthyl reaction is anticipated to be the fastest, while the total rate constants for acenaphthylene + 4-phenanthrenyl and acepyrene + pyrenyl appeared to be similar. This result is not surprising since acenaphthylene + 1-naphthyl is controlled by a submerged entrance barrier, whereas the barriers for the other two reactions are both close to 1 kcal/mol. In the acenaphthylene + 1-naphthyl reaction, the formation of the thermalized adduct W1 is preferable up to 1375 K and at higher temperatures, when W1 is no longer stable, the formation of the C-C covalently bound product P2 is more favorable than the formation of the E-bridged product P1. While W1 predominantly dissociates to P1 + H (Fig. 4(b)), both P1 and P2 formed from acenaphthylene + 1-naphthyl appeared to be rather unstable with respect to their reverse reactions with an H atom. As seen in Figs. 4(c) and 4(d), both P1 + H and P2 + H generally have higher total rate constants (in the temperature range of interest, above 1000 K) than that for acenaphthylene + 1-naphthyl. In the P1 + H reaction, collisional stabilization of W1 is preferred up to 1375 K and at higher temperatures, the reaction forms the initial reactants and P2 + H in ratios of 1.60-1.75 to 1. On the other hand, the P2 + H reaction is dominated by the formation of acenaphthylene + 1-naphthyl above 1375 K.

The picture is quite distinct for the acenaphthylene + 4-phenanthrenyl reaction. The forward reaction produces the E-bridged product P1 + H with the branching ratio of over 50% in the 1000-2250 K range and 98-81% at T = 1250-1800 K. At lower temperatures, collisional stabilization of a more stable W2 intermediate is significant, which persists up to 1125 K. At higher temperatures, the formation of P2 + H becomes more favorable due to its entropic preference but the relative yield of P2 overtakes that of P1 only above 2250 K. The adduct W2 nearly exclusively decomposes to P1 + H (Fig. 4(b)). The reverse reaction P1 + H forms almost only W2 up to 1125 K and at higher temperatures produces the initial reactants acenaphthylene + 4-phenanthrenyl and P2 + H in ratios of 5.1-4.5 to 1 (Fig. 4(c)). A peculiar kink is seen on the graph of the total P1 + H rate constant, which drops between 1125 and 1250 K and then begins rising again at higher temperature. This is a result of a typical fall-off behavior when the W2 intermediate becomes unstable and dissociates preferably back to P1 + H rather than proceeding forward to acenaphthylene + 4-phenanthrenyl or P2 + H. As the temperature increases, the latter two

decomposition channels of W2 become increasingly more favorable as compared the reverse reaction back to P1 + H and the total phenomenological rate constant of P1 + H rises. The P2 + H reaction produces mostly P1 + H up to ~1700 K and in the 1800-2500 K, the branching ratio of acenaphthylene + 4-phenanthrenyl grows to 54-86%.

The overall propensity to form the E-bridged product P1 in the three considered dimerization reactions can be assessed by looking at the equilibrium constants K_{eq} for the reactants (R) = P1 + H, R = P2 + H, and P1 + H = P2 + H reactions (Fig. 5). For R = P1 + H (Fig. 5(a)), K_{eq} is maximal for acepyrene + pyrenyl closely followed by acenaphthylene + 4-phenanthrenyl and minimal for acenaphthylene + 1-naphthyl. For instance, at 1500 K the respective values are 0.24, 0.17, and 0.07 and at 1650 K, they are 0.13, 0.09, and 0.04. On the other hand, the plot of K_{eq}(R = P2 + H) (Fig. 5(b)) shows that the formation of the C-C covalently bound product P2 is more favorable in the acenaphthalene + 1-naphthyl reaction, whereas it is very unlikely for acenaphthylene + 4-phenanthrenyl and acepyrene + pyrenyl. The conversion of the E-bridged dimer P1 to the covalently bound structure P2 is again most favorable for acenaphthylene + 1-naphthyl but above 1800 K becomes preferable for the other two reactions (Fig. 5(c)). Nevertheless, as seen in Fig. 5(b), at these high temperatures, the equilibrium between P2 and R is strongly shifted toward the reactants, i.e., the dimer formation is unlikely. In summary, this consideration in terms of the thermodynamic equilibrium shows that the tendency to form the E-bridged dimer is higher for a bay PAH edge (as in 4-phenanthrenyl) than for a zigzag edge (as in 1-naphthyl) and grows with the size of the PAH molecules involved (e.g., in going from acenaphthylene + 1-naphthyl to acepyrene + pyrenyl). Also, at temperatures above 1800 K, the E-bridge dimerization reaction is thermodynamically unlikely.

Nucleation flux

The nucleation fluxes were calculated for the same flame environment and following the same theoretical framework that was used in the prior study.[4] The nucleation was represented by a consecutive series of a two-step HACA sequence,

$$P_i + H \Leftrightarrow P_i\bullet + H_2 \quad \text{(Ia)}$$

$$P_i\bullet + H \Leftrightarrow P_i \quad \text{(Ib)}$$

$$P_i\bullet + P_{mono} \Leftrightarrow P_{i+1} + H, \quad \text{(II)}$$

for i = 1, 2, …, 100. Step (I), composed of reactions (Ia) and (Ib), is the ‘‘pushing’’ activation (de-activation) of PAH cluster P_i through H abstraction (H-addition) and step (II) is the ‘‘pulling’’ carbon addition.[2,4,5] Reaction (Ia) is the H-abstraction from a bay C–H site of the aromatic edge, P_{mono} is the monomer PAH with a five-member ring (e.g., acepyrene, A4R5, or acenaphthylene, A2R5), and reaction (II) is the 5-6 E-bridge formation, taking place in a rotationally activated collision of $P_i\bullet$ and P_{mono}. The reaction model (I)-(II) was applied to several cases; they are

described in the following paragraphs and detail the assignment of reactants P_i, P_i•, and P_{mono}. It is also pertinent to mention that, similar to the prior study,[4] the maximum value of *i* set to 100 assured that the termination of the reversible sequence does not affect the phenomenon of interest, which is governed by the computed profiles of the initial polymers.

The per-site reaction rate coefficient for reaction (Ia) and its reverse were taken from a recent study[27] and that of reaction (Ib) from Harding et al.[28] The forward rate of reaction (Ia) was calculated by multiplying its per-site rate coefficient by the number of available for reaction (Ia) sites on the outer edges of the PAH cluster, P_i.

Allowing for reaction (II) to proceed with the rate constant values computed in the present study, i.e. without considering rotational excitation, produced no nucleation fluxes, as demonstrated by the black dashed line in Fig. 6 for the 1-naphthyl + acenaphthylene (A2-1 + A2R5) system. With the assumption of rotational excitation, following Ref. 4, all present systems exhibited nucleation behavior to one extent or another; the numerical results are presented in Fig. 6. Under this assumption, the forward direction of reaction (II) was assigned the collisional rate and its reverse rate was evaluated with the reaction rate coefficient computed in the present study. The extent of the nucleation flux was assessed by comparison of the developing cluster distributions with those of irreversible polymerization of pyrene (blue solid line in Fig. 6) and the pyrenyl + acepyrene one examined in the prior study[4] (brown solid line in Fig. 6), as the latter two cases bracket the range of meaningful nucleation fluxes.[4]

We started the analysis by considering the 5-6 E-bridge-forming system of P_1 being phenanthrene (A3) and P_{mono} acepyrene (A4R5). The development of internal rotation in the collision of 4-phenanthrenyl (A3-4) with acepyrene is expected to be close to that of the pyrenyl (A4-) + acepyrene system in light of the similarity in the molecular structure and size of the colliding partners and considering the similarity of molecular-dynamic results of phenanthrene[29] and pyrene[30] dimerizations. For the present simulation, we assumed the rate coefficient of the reverse of reaction (II) to be that of the reverse of the 4-phenanthrenyl + acenaphthylene reaction computed in the present study. Such an assumption is warranted by the fact that our preliminary B3LYP/6-311G(d,p) calculations of the PES for the 4-phenanthrenyl + acepyrene reaction gave the energies of all intermediates and transition states within 0.2-0.3 kcal/mol from the corresponding energies in the 4-phenanthrenyl + acenaphthylene system. Moreover, the energy of the E-bridged P1 + H product of 4-phenanthrenyl + acepyrene at the G3(CC,MP2) level, -26.5 kcal/mol, closely matches the energy of P1 + H in the 4-phenanthrenyl + acenaphthylene reaction, -26.2 kcal/mol. The computed P_i distribution of the 5-6 case, displayed by the yellow solid line in Fig. 6, is initially slightly higher than the 5-5 A4- + A4R5 case, due to the higher initial concentration of P_1, but then approaches the 5-5 case, due to higher reverse rate of step (II).

Interestingly, combining the new 5-6 and previous 5-5 growth mechanisms showed a stronger nucleation. In this case, the growth sequence began with 4-phenanthrenyl + acepyrene step. The formed 5-6 E-bridge structure does not have bay sites and hence the next E-bridge-forming step was acepyrene (the monomer) reacting at its zigzag site, i.e., the 5-5 mechanism of the prior study.[4] These reaction steps then were repeated/combined for the rest of the growth sequence. The computed P_i distribution in this case, displayed by the red line marked with asterisks in Fig. 6, retains the strength of the 5-6 model for the initial clusters yet converges now to the irreversible pyrene case. Since the latter has been shown to reproduce soot inception observed in flames (e.g., Refs. 24 and 31), the obtained here computational result signifies that a rotationally-excited E-bridge formation by a mix of 5-6 and 5-5 steps is a mechanism quantitatively consistent with these observations. The exact numerical outcome should be determined by steric opportunities presented for the zigzag versus bay sites.

Assuming acenaphthylene instead of acepyrene being the monomer for the purely 5-6 growth system, i.e. P_1 = A3-4 and P_{mono} = A2R5, resulted in the nucleation flux that is similar to the one obtained with the combined 5-6 and 5-5 systems (displayed by the green line marked with open circles in Fig. 6). However, the lifetime of a rotationally-excited adduct, if developed, should be shorter in this case of a smaller colliding partner. All the more so for the case of the 1-naphthyl + acenaphthylene system. Its purely chemical reaction, as mentioned above, does not develop the nucleation flux. A "formal" simulation assuming the rotationally-activated mechanism produces a stronger nucleation flux than the irreversible pyrene system (not shown in Fig. 6). However, the development of internal rotation for a sufficiently long time in the 1-naphthyl + acenaphthylene system is at question given the much lower interaction energy.[32] Thus, both of these A2R5 systems need to be examined in a non-equilibrium setting.

Conclusions

Considered as individual steps, the two-ring reaction systems examined in the present study are computed to have faster forward rates but lower equilibrium constants than the four-ring systems.

Compared at the same size, the formation of the E-bridge structures at the bay radical sites are faster than at the zigzag radical sites. On their own, the bay-forming E-bridges lead to the increased nucleation rates, as compared to the zigzag-forming ones, for acenaphthylene but not for acepyrene. However, the rotationally-activated dimerization for acenaphthylene could be less likely to develop, and the purely chemical reaction path does not lead to any nucleation. Yet, a model combining both the bay and zigzag rotationally-induced formation of E-bridges is successful to reach the level of nucleation fluxes comparable to those of the irreversible pyrene

dimerization. The latter result affirms the rotationally-activated dimerization as a feasible mechanism for soot particle nucleation introduced in the prior study.[4] In future studies, the monomer size effect on the kinetics of the rotationally-activated dimerization involving the E-bridge formation should be systematically investigated through chemically accurate calculations of the relevant PES and reaction rate constant, such as e.g., for acepyrene + 4-phenanthrenyl. These studies would then allow us to address the question at what size PAH molecules begin forming three-dimensional clusters leading to soot particle inception.

Conflicts of interest

There are no conflicts to declare.

Acknowledgements

The work at Samara University was supported by the grant from the Russian Science Foundation (project No. 19-73-00316). The work at Florida International University was funded by the US Department of Energy, Basic Energy Sciences DE-FG02-04ER15570. A.M.M. also acknowledges the Instructional & Research Computing Center (IRCC, web: http://ircc.fiu.edu) at FIU for providing HPC computing resources that have contributed to the research results reported within this paper.

Figure Captions

Figure 1. Illustration of the 5-5 (left) and 5-6 (right) E-bridge molecular structures.

Figure 2. PAH distribution obtained in KMC simulations for the conditions of a burner-stabilized stagnation flame:[8] 16.3% C_2H_4–23.7% O_2–Ar, cold gas velocity 8.0 cm/s, and burner-to-stagnation surface separation 0.8 cm. The gas-phase composition was computed with the ABF model.[24] 1000 KMC runs were performed starting at 1300 K position of the flame with a pyrene substrate.

Figure 3. Potential energy diagrams of the acenaphthylene + 1-naphthyl (top), acepyrene + pyrenyl (middle), and acenaphthylene + 4-phenanthrenyl (bottom) calculated at the G3(MP2,CC)//B3LYP/6-311G(d,p) + ZPE(B3LYP/6-311G(d,p)) level of theory. Relative energies in kcal/mol are shown with respect to the initial reactants. For the acepyrene + pyrenyl system,[4] some relative energies (shown in italics) were computed at the B2PLYPD3/cc-pVTZ//B3LYP/6-311G(d,p) + ZPE(B3LYP/6-311G(d,p)) level of theory.

Figure 4. Forward and reverse rate constants for the acenaphthylene + 1-naphthyl (dashed lines), acepyrene + pyrenyl (dotted lines, from Ref. 4), and acenaphthylene + 4-phenanthrenyl (solid lines) reactions calculated using the RRKM-ME approach: (a) forward reactions; (b) decomposition of the W1 adduct (W2 for acenaphthylene + 4-phenanthrenyl); (c) reverse P1 + H reactions; (d) reverse P2 + H reactions.

Figure 5. Calculated equilibrium constants K_{eq} for the acenaphthylene + 1-naphthyl (dashed lines), acepyrene + pyrenyl (dotted lines, from Ref. 4), and acenaphthylene + 4-phenanthrenyl (solid lines) reactions: (a) Reactants (R) = P1 + H; (b) R = P2 + H; (c) P1 + H = P2 + H.

Figure 6. P_i distributions computed with the nucleation model for the midpoint of the flame simulation, 5 ms.

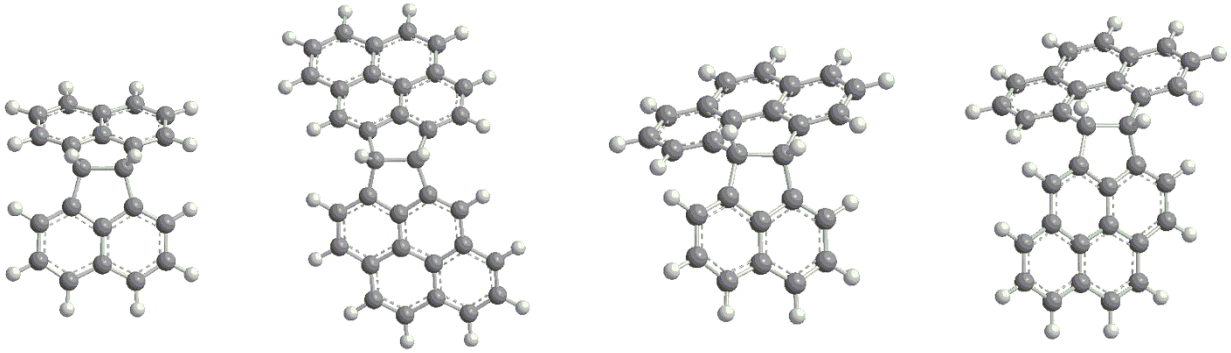

5-5 E-bridge **5-6 E-bridge**

Figure 1

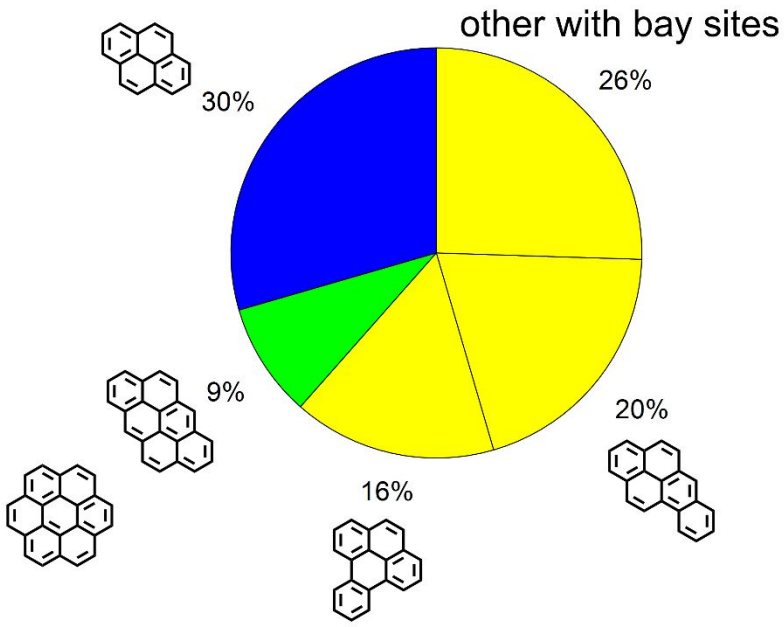

Figure 2

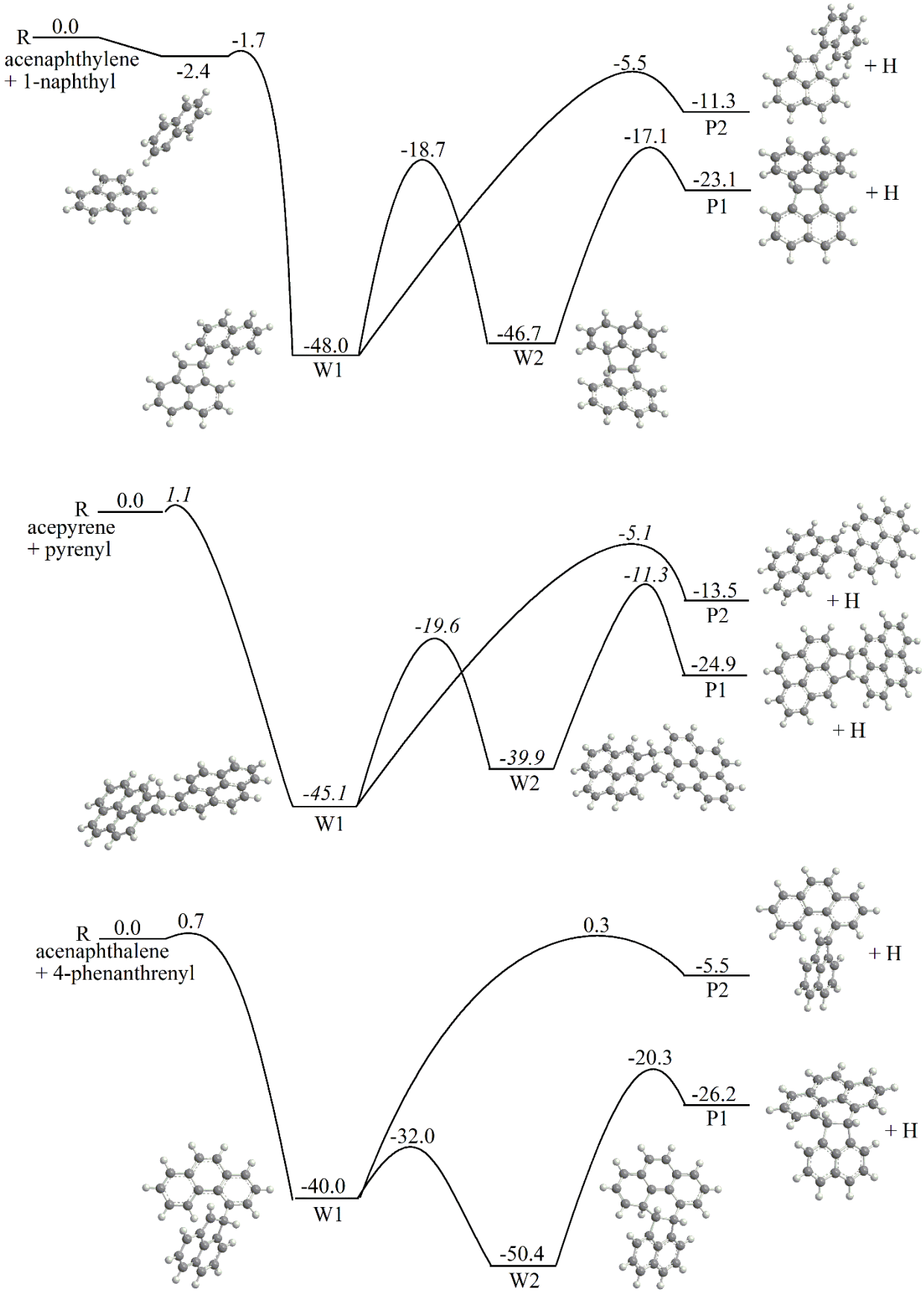
R
0.0
acenaphthylene
+ 1-naphthyl
-2.4
-1.7
-48.0
W1
-18.7
-46.7
W2
-5.5
-11.3
P2
-17.1
-23.1
P1
+ H
+ H
R
0.0
1.1
acepyrene
+ pyrenyl
-45.1
W1
-19.6
-39.9
W2
-5.1
-11.3
-13.5
P2
-24.9
P1
+ H
+ H
R
0.0
0.7
acenaphthalene
+ 4-phenanthrenyl
-40.0
W1
-32.0
-50.4
W2
0.3
-5.5
P2
-20.3
-26.2
P1
+ H
+ H

Figure 3

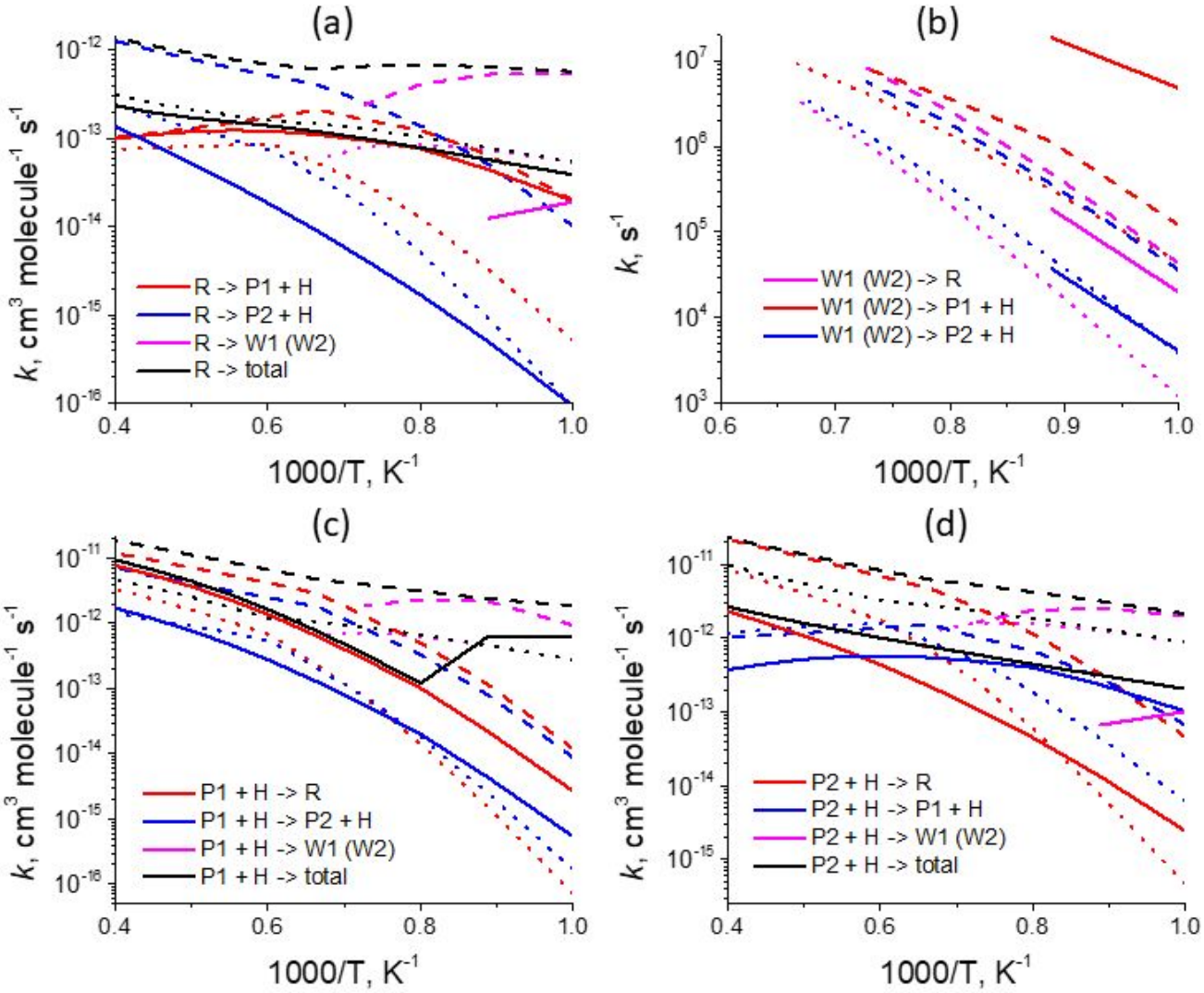
(a)
k, cm3 molecule-1 s-1
R -> P1 + H
R -> P2 + H
R -> W1 (W2)
R -> total
1000/T, K-1
(b)
k, s-1
W1 (W2) -> R
W1 (W2) -> P1 + H
W1 (W2) -> P2 + H
1000/T, K-1
(c)
k, cm3 molecule-1 s-1
P1 + H -> R
P1 + H -> P2 + H
P1 + H -> W1 (W2)
P1 + H -> total
1000/T, K-1
(d)
k, cm3 molecule-1 s-1
P2 + H -> R
P2 + H -> P1 + H
P2 + H -> W1 (W2)
P2 + H -> total
1000/T, K-1

Figure 4

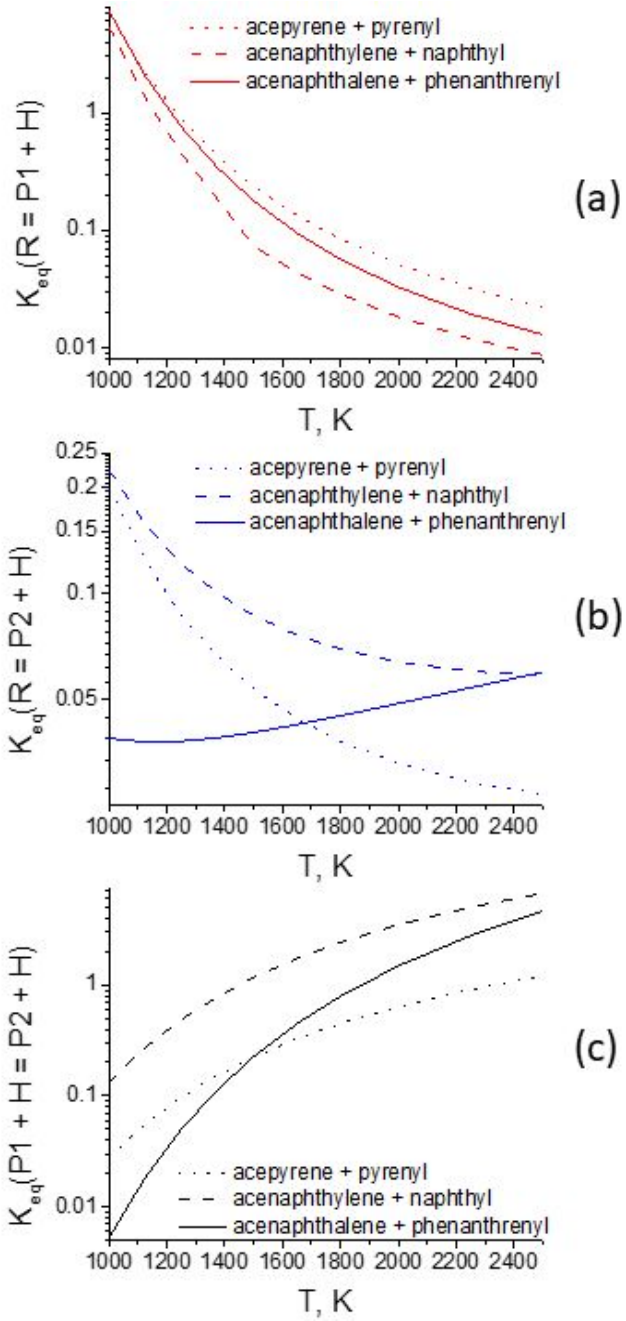
acepyrene + pyrenyl
acenaphthylene + naphthyl
acenaphthalene + phenanthrenyl
K_{eq}(R = P1 + H)
1
0.1
0.01
1000 1200 1400 1600 1800 2000 2200 2400
T, K
(a)
0.25
0.2
0.15
0.1
0.05
K_{eq}(R = P2 + H)
(b)
K_{eq}(P1 + H = P2 + H)
(c)

Figure 5

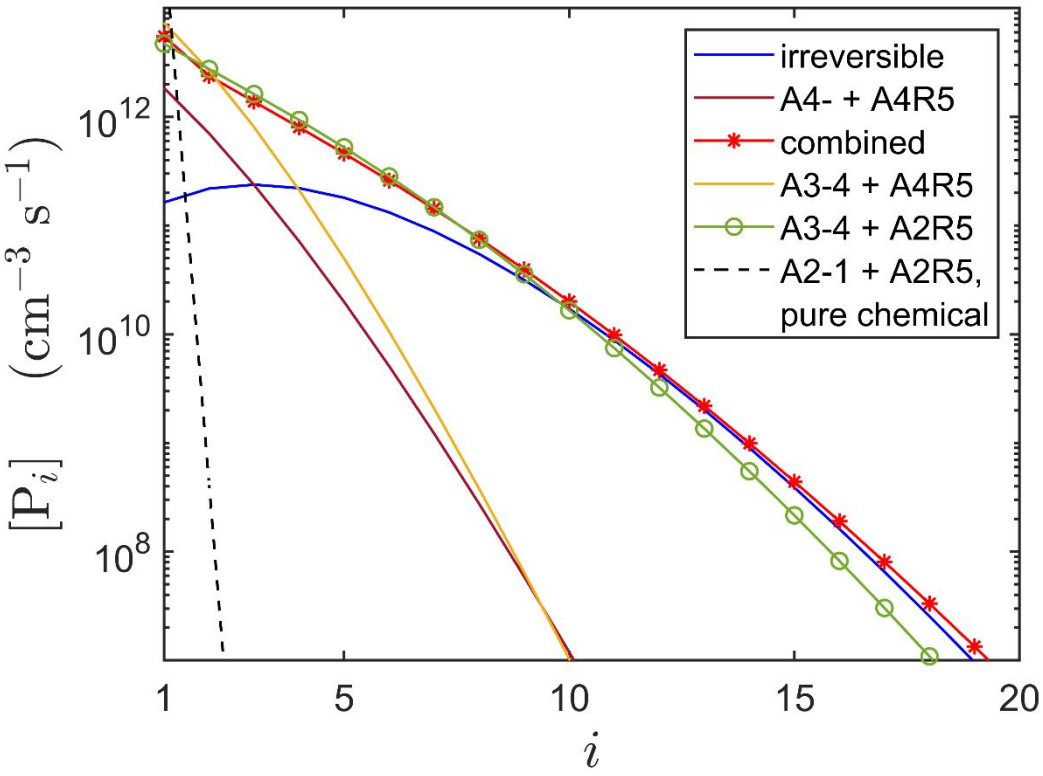
irreversible
A4- + A4R5
combined
A3-4 + A4R5
A3-4 + A2R5
A2-1 + A2R5, pure chemical
$[P_i]$ $(cm^{-3}\ s^{-1})$
10^{12}
10^{10}
10^{8}
1
5
10
15
20
i

Figure 6

References

1 B. S. Haynes and H. Gg. Wagner, Soot formation, *Prog. Energy Combust. Sci.*, 1981, **7**, 229–273.

2 M. Frenklach, Reaction mechanism of soot formation in flames, *Phys. Chem. Chem. Phys.*, 2002, **4**, 2028–2037.

3 H. Wang, Formation of nascent soot and other condensed-phase materials in flames, *Proc. Combust. Inst.*, 2011, **33**, 41–67.

4 M. Frenklach and A. M. Mebel, On the mechanism of soot nucleation, *Phys. Chem. Chem. Phys.*, 2020, **22**, 5314–5331.

5 M. Frenklach, D. W. Clary, W. C. Gardiner and S. E. Stein, Detailed kinetic modeling of soot formation in shock-tube pyrolysis of acetylene, *Symp. (Int.) Combust.*, 1985, **20**, 887–901.

6 S. E. Stein and A. Fahr, High-temperature stabilities of hydrocarbons, *J. Phys. Chem.*, 1985, **89**, 3714–3725.

7 B. D. Adamson, S. A. Skeen, M. Ahmed and N. Hansen, Detection of Aliphatically Bridged Multi-Core Polycyclic Aromatic Hydrocarbons in Sooting Flames with Atmospheric-Sampling High-Resolution Tandem Mass Spectrometry, *J. Phys. Chem. A*, 2018, **122**, 9338–9349.

8 A. D. Abid, J. Camacho, D. A. Sheen and H. Wang, Quantitative measurement of soot particle size distribution in premixed flames - The burner-stabilized stagnation flame approach, *Combust. Flame*, 2009, **156**, 1862–1870.

9 C. Lee, W. Yang and R. G. Parr, Development of the Colle-Salvetti correlation-energy formula into a functional of the electron density, *Phys. Rev. B*, 1988, **37**, 785–789.

10 A. D. Becke, Density-functional thermochemistry. III. The role of exact exchange, *J. Chem. Phys.*, 1993, **98**, 5648–5652.

11 M. J. Frisch, G. W. Trucks, H. B. Schlegel, G. E. Scuseria, M. A. Robb, J. R. Cheeseman, G. Scalmani, V. Barone, B. Mennucci, G. A. Petersson, H. Nakatsuji, M. Caricato, X. Li, H. P. Hratchian, A. F. Izmaylov, J. Bloino, G. Zheng, L. Sonnenberg, M. Hada, M. Ehara, K. Toyota, R. Fukuda, J. Hasegawa, M. Ishida, T. Nakajima, Y. Honda, H. Nakai, T. Vreven, J. A. Montgomery, J. E. Peralta, F. Ogliaro, M. Bearpark, J. J. Heyd, E. Brothers, K. N. Kudin, V. N. Staroverov, T. Keith, R. Kobayashi, J. Normand, K. Raghavachari, A. Rendell, J. C. Burant, S. S. Iyengar, J. Tomasi, M. Cossi, N. Rega, J. M. Millam, M. Klene, J. E. Knox, J. B. Cross, V. Bakken, C. Adamo, J. Jaramillo, R. Gomperts, R. E. Stratmann, O. Yazyev, A. J. Austin, R. Cammi, C. Pomelli, J. W. Ochterski, R. L. Martin, K. Morokuma, V. G. Zakrzewski, G. A. Voth, P. Salvador, J. J. Dannenberg, S. Dapprich, A. D. Daniels, O. Farkas, J. B. Foresman, J. V. Ortiz, J. Cioslowski and D. J. Fox, *Gaussian 09*, 2010.

12 A. G. Baboul, L. A. Curtiss, P. C. Redfern and K. Raghavachari, Gaussian-3 theory using density functional geometries and zero-point energies, *J. Chem. Phys.*, 1999, **110**, 7650–7657.

13 L. A. Curtiss, P. C. Redfern, K. Raghavachari, V. Rassolov and J. A. Pople, Gaussian-3 theory using reduced Mo/ller-Plesset order, *J. Chem. Phys.*, 1999, **110**, 4703–4709.

14 L. A. Curtiss, K. Raghavachari, P. C. Redfern, A. G. Baboul and J. A. Pople, Gaussian-3 theory using coupled cluster energies, *Chem. Phys. Lett.*, 1999, **314**, 101–107.

15 H.-J. Werner, P. J. Knowles, G. Kinizia, F. R. Manby, M. Schutz, P. Celani, T. Korona and R. Lindh, *MOLPRO*, 2010.

16 Y. Georgievskii, J. A. Miller, M. P. Burke and S. J. Klippenstein, Reformulation and Solution of the Master Equation for Multiple-Well Chemical Reactions, *J. Phys. Chem. A*, 2013, **117**, 12146–12154.

17 Y. Georgievskii and S. J. Klippenstein, *Master Equation System Solver (MESS)*, 2015, available on line at https://github.com/PACChem/MESS.

18 H. Wang and M. Frenklach, Transport properties of polycyclic aromatic hydrocarbons for flame modeling, *Combust. Flame*, 1994, **96**, 163–170.

19 A. Vishnyakov, P. G. Debenedetti and A. V. Neimark, Statistical geometry of cavities in a metastable confined fluid, *Phys. Rev. E*, 2000, **62**, 538–544.

20 P. I. Ravikovitch, A. Vishnyakov and A. V. Neimark, Density functional theories and molecular simulations of adsorption and phase transitions in nanopores, *Phys. Rev. E*, 2001, **64**, 011602.

21 J. Troe, Theory of thermal unimolecular reactions at low pressures. I. Solutions of the master equation, *J. Chem. Phys.*, 1977, **66**, 4745–4757.

22 A. W. Jasper and J. A. Miller, Theoretical Unimolecular Kinetics for CH4 + M ⇄ CH3 + H + M in Eight Baths, M = He, Ne, Ar, Kr, H2, N2, CO, and CH4, *J. Phys. Chem. A*, 2011, **115**, 6438–6455.

23 D. G. Goodwin, H. K. Moffat and R. L. Speth, *Cantera: An Object-oriented Software Toolkit for Chemical Kinetics, Thermodynamics, and Transport Processes. Version 2.3.0*, Zenodo, 2017.

24 J. Appel, H. Bockhorn and M. Frenklach, Kinetic modeling of soot formation with detailed chemistry and physics: laminar premixed flames of C2 hydrocarbons, *Combust. Flame*, 2000, **121**, 122–136.

25 R. Whitesides and M. Frenklach, Detailed Kinetic Monte Carlo Simulations of Graphene-Edge Growth, *J. Phys. Chem. A*, 2010, **114**, 689–703.

26 M. Frenklach, Z. Liu, R. I. Singh, G. R. Galimova, V. N. Azyazov and A. M. Mebel, Detailed, sterically-resolved modeling of soot oxidation: Role of O atoms, interplay with particle

nanostructure, and emergence of inner particle burning, *Combust. Flame*, 2018, **188**, 284–306.

27 A. S. Semenikhin, A. S. Savchenkova, I. V. Chechet, S. G. Matveev, Z. Liu, M. Frenklach and A. M. Mebel, Rate constants for H abstraction from benzo(a)pyrene and chrysene: a theoretical study, *Phys. Chem. Chem. Phys.*, 2017, **19**, 25401–25413.

28 L. B. Harding, Y. Georgievskii and S. J. Klippenstein, Predictive Theory for Hydrogen Atom−Hydrocarbon Radical Association Kinetics, *J. Phys. Chem. A*, 2005, **109**, 4646–4656.

29 M. Wei, S. Wu, F. Li, D. Zhang, T. Zhang and G. Guo, Molecular modelling investigations on the possibility of phenanthrene dimers to be the primary nuclei of soot, *Combust. Theor. Model.*, 2017, **21**, 1189–1198.

30 C. A. Schuetz and M. Frenklach, Nucleation of soot: Molecular dynamics simulations of pyrene dimerization, *Proc. Combust. Inst.*, 2002, **29**, 2307–2314.

31 D. Hou, C. S. Lindberg, M. Y. Manuputty, X. You and M. Kraft, Modelling soot formation in a benchmark ethylene stagnation flame with a new detailed population balance model, *Combust. Flame*, 2019, **203**, 56–71.

32 N. J. Silva, F. B. C. Machado, H. Lischka and A. J. A. Aquino, π–π stacking between polyaromatic hydrocarbon sheets beyond dispersion interactions, *Phys. Chem. Chem. Phys.*, 2016, **18**, 22300–22310.

TOC Graphic

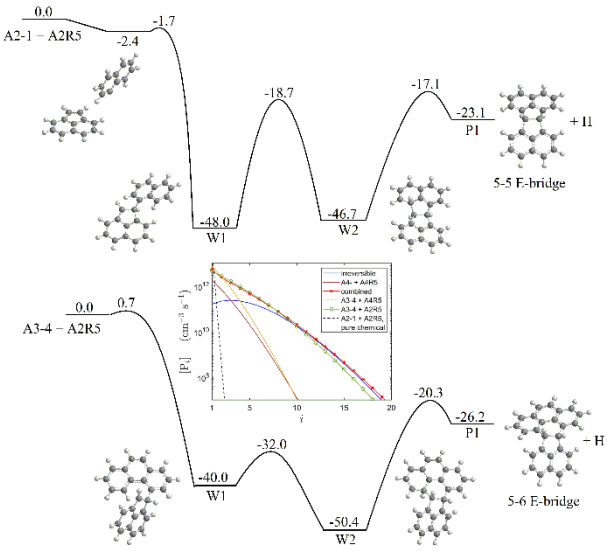

A model combining both the bay and zigzag rotationally-induced formation of E-bridges between PAH molecules increases nucleation rates and affirms the rotationally-activated dimerization as a feasible mechanism for soot particle nucleation.

TOC Graphic

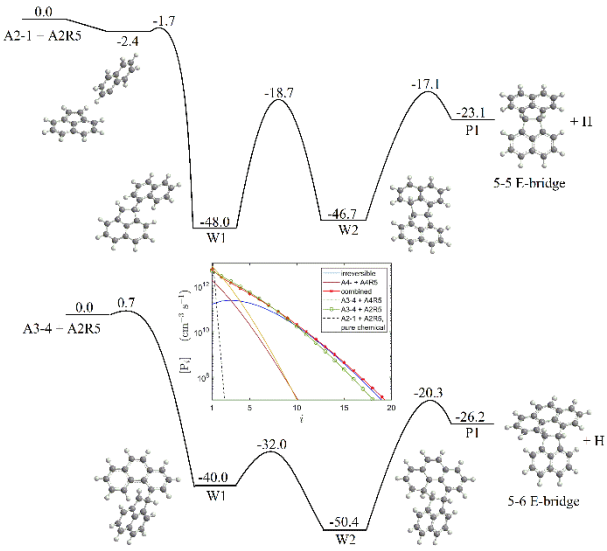

A model combining both the bay and zigzag rotationally-induced formation of E-bridges between PAH molecules increases nucleation rates and affirms the rotationally-activated dimerization as a feasible mechanism for soot particle nucleation.